The Astrophysical Journal, 675:1518–1530, 2008 March 10

ORBITAL PARAMETERS AND CHEMICAL COMPOSITION OF FOUR WHITE DWARFS IN POST–COMMON-ENVELOPE BINARIES

Adela Kawka,[1] Stéphane Vennes,[2] Jean Dupuis,[3] Pierre Chayer,[4] and Thierry Lanz[5]

Received 2007 July 14; accepted 2007 November 9

ABSTRACT

We present *FUSE* observations of the hot white dwarfs in the post–common-envelope binaries Feige 24, EUVE J0720−317, BPM 6502, and EUVE J2013+400. The spectra show numerous photospheric absorption lines, which trace the white dwarf orbital motion. We report the detection of C III, O VI, P V, and Si IV in the spectra of Feige 24, EUVE J0720−317, and EUVE J2013+400 and the detection of C III, N II, Si III, Si IV, and Fe III in the spectra of BPM 6502. Abundance measurements support the possibility that white dwarfs in post–common-envelope binaries accrete material from the secondary star wind. The *FUSE* observations of BPM 6502 and EUVE J2013+400 cover a complete binary orbit. We used the *FUSE* spectra to measure the radial velocities traced by the white dwarf in the four binaries, where the zero-point velocities were fixed using the ISM velocities in the line of sight of the stellar systems. For BPM 6502 we determined a white dwarf velocity semiamplitude of $K_{\rm WD} = 18.6 \pm 0.5$ km s^{-1}, and with the velocity semiamplitude of the red dwarf companion ($K_{\rm RD} = 75.2 \pm 3.1$ km s^{-1}), we estimate the mass ratio to be $q = 0.25 \pm 0.01$. Adopting a spectroscopic mass determination for the white dwarf, we infer a low secondary mass of $M_{\rm RD} = 0.14 \pm 0.01\ M_{\odot}$. For EUVE J2013+400 we determine a white dwarf velocity semiamplitude of $K_{\rm WD} = 36.7 \pm 0.7$ km s^{-1}. The *FUSE* observations of EUVE J0720−317 cover approximately 30% of the binary period and, combined with the *HST* GHRS measurements, we update the binary properties. *FUSE* observations of Feige 24 cover approximately 60% of the orbit, and we combine this data set with *HST* STIS data to update the binary properties.

Subject headings: binaries: spectroscopic — stars: abundances — white dwarfs

Online material: color figures

1. INTRODUCTION

Post–common-envelope binaries consist of an evolved primary (white dwarf or sdB) and a late-type main-sequence secondary in close orbit. These binaries are thought to have evolved from wide binary systems, where the more massive star evolved off the main sequence, filling its Roche lobe and beginning mass transfer onto its less massive companion. If the transfer is dynamically unstable, a common envelope (CE) is formed, and friction between the stellar components and the CE decreases the orbital separation and induces the ejection of the CE. Depending on the separation of the components, some of these systems further evolve to become cataclysmic variables. From the sample of well-studied post-CE binaries (Schreiber & Gänsicke 2003), approximately half will evolve into cataclysmic variables within a Hubble time.

The atmosphere of a white dwarf a in a close binary system usually contains enhanced traces of heavy elements. Vennes et al. (1999) found that the large abundance of carbon and helium, as well as time-variable helium abundance, in some white dwarfs provides evidence for ongoing accretion from the red dwarf.

We present high-resolution far-ultraviolet (FUV) spectroscopic observations of Feige 24 (PG 0232+035: Vennes & Thorstensen 1994b; Vennes et al. 2000), WD 0718−316 (EUVE J0720−317, 2RE J0720−318: Vennes & Thorstensen 1994a; Barstow et al. 1995a), WD 1042−690 (BPM 6502: Kawka et al. 2000), and WD 2011+398 (EUVE J2013+400, 2RE J2013+400: Thorstensen et al. 1994; Barstow et al. 1995b) in § 2. We present the analyses of the *Far-Ultraviolet Spectroscopic Explorer* (*FUSE*) spectra in § 3, determine new orbital and stellar parameters of the four binary systems in § 4, and measure the heavy-element abundance in the white dwarf atmospheres in § 5. We summarize in § 6.

2. OBSERVATIONS

We have obtained high-resolution FUV spectra of four close binary systems with *FUSE* (Table 1). The spectrograph covers the FUV spectral range from 905 to 1187 Å with a spectral resolution $R = 20,000 \pm 2000$. The instruments are described in detail by Moos et al. (2000) and Sahnow et al. (2000a, 2000b). The observations were made using the LWRS (EUVE J0720−317, BPM 6502, and EUVE J2013+400) and MDRS (Feige 24 and EUVE J2013+400) apertures in time-tagged mode, except for Feige 24, which was observed in the HIST mode. The data for EUVE J0720−317 and BPM 6502 were processed with the CALFUSE pipeline version 3.1, and the data for Feige 24 and EUVE J2013+400 were processed with the CALFUSE pipeline version 3.0. For the abundance analysis, we co-added the individual exposures after aligning them on the photospheric lines using the calculated radial velocities. Figure 1 shows the *FUSE* spectra of Feige 24, EUVE J0720−317, BPM 6502, and EUVE J2013+400, indicating key heavy elements. Table 2 lists important photospheric lines in Feige 24, EUVE J0720−317, and EUVE J2013+400, while Table 3 lists important lines in BPM 6502.

3. WHITE DWARF ATMOSPHERIC PARAMETERS

The *FUSE* spectrum of Feige 24 was analyzed by Vennes et al. (2005). Using LTE models, they determined an effective temperature

[1] Astronomický ústav AV ČR, Fričova 298, CZ-251 65 Ondřejov, Czech Republic; kawka@sunstel.asu.cas.cz.
[2] Department of Physics and Space Sciences, Florida Institute of Technology, Melbourne, FL 32901; svennes@fit.edu.
[3] Canadian Space Agency, 6767 Route de l'Aeroport, Saint-Hubert, QC J3Y 8Y9, Canada; jean.dupuis@space.gc.ca.
[4] Department of Physics and Astronomy, Johns Hopkins University, Baltimore, MD 21218; chayer@pha.jhu.edu.
[5] Department of Astronomy, University of Maryland, College Park, MD 20742; tlanz@umd.edu.

TABLE 1
FUSE Observation Log

Date	Exposure Time (s)	Aperture	Data Set	Observer
		Feige 24		
2003 Dec 7	2149	MDRS	P1040501	Moos
2004 Jan 2.....	16117	MDRS	P1040503	Moos
2004 Jan 6.....	11999	MDRS	P1040504	Moos
		EUVE J0720−317		
2001 Nov 13.....	17700	LWRS	B0510101	Vennes
		BPM 6502		
2002 Jun 26	32100	LWRS	Z9104501	Andersson
2006 Jan 21.....	10696	LWRS	U1074601	Blair
2006 Jan 22.....	7122	LWRS	U1074602	Blair
2007 Mar 2	12758	LWRS	U1074604	Blair
		EUVE J2013+400		
2000 Oct 11	11200	LWRS	P2040401	Moos
2002 Oct 29	6543	LWRS	M1053101	Dupuis
2003 Oct 21	42607	MDRS	D0580101	Vidal-Madjar
2003 Oct 23	12881	LWRS	M1053102	Dupuis

of 64,700 ± 3000 K and $\log g = 7.58 \pm 0.25$. Vennes et al. (2005) also investigated the effect of using LTE models on temperatures and surface gravities obtained from the analysis of Lyman and Balmer lines of hot white dwarfs. They found that for objects hotter than 50,000 K, assuming low metallicity, the LTE determinations are overestimated by approximately 4000 K. Using the NLTE correction vector, the temperature would be revised to approximately 60,000 K, which within the uncertainties is in agreement with previous temperature determinations, and in this work we will assume an effective temperature of $T_{\rm eff} = 57{,}000 \pm 2000$ K, which is based on estimates from previous spectroscopic studies (e.g., Vennes & Lanz 2001).

The *FUSE* spectrum of BPM 6502 displays Lyβ and Lyγ satellites. Hébrard et al. (2003) compared the *FUSE* spectrum to a LTE model spectrum at $T_{\rm eff} = 21{,}380$ and $\log g = 7.86$ that included the quasi-molecular satellites of Lyα, Lyβ, and Lyγ. The theoretical spectrum showed reasonably good agreement with the observed *FUSE* spectrum of BPM 6502; however, some discrepancies are observed. Hébrard et al. (2003) noted that their models do not include the variation of the dipole moment during the collision, which may have a significant effect on the strengths of the satellite profiles. In this work, we adopt the effective temperature and surface gravity determined by Kawka et al. (2007). Even though these parameters were determined using optical spectra, only Hα is significantly contaminated and as a result was excluded in their analysis.

We used the *FUSE* spectra to obtain an effective temperature, surface gravity, and helium abundance of the white dwarfs in EUVE J0720−317 and EUVE J2013+400. We computed a grid of LTE plane-parallel models. The grid of models extends from $T_{\rm eff} = 30{,}000$ to 70,000 K (in steps of 4000 K), from $\log g =$ 7.0 to 9.5 (in steps of 0.25 dex), and from $\log(N_{\rm He}/N_{\rm H}) = -4.0$ to 0.0 (in steps of 0.5 dex). We fitted six channels (SIC1B, SIC2A, LIF2B, LIF1A, SIC1A, and SIC2B) simultaneously using a χ^2 minimization technique to obtain an effective temperature, surface gravity, and helium abundance. Regions that show interstellar absorption features were excluded from the fit. We obtained $T =$ $52{,}750 \pm 150$, $\log g = 7.73 \pm 0.03$, and $\log(N_{\rm He}/N_{\rm H}) = -3.28 \pm$ 0.08 for EUVE J0720−317. For EUVE J2013+400 we obtained $T = 47{,}800 \pm 200$, $\log g = 8.20 \pm 0.03$, and $\log(N_{\rm He}/N_{\rm H}) =$ -2.90 ± 0.08. The atmospheric parameters derived from *FUSE* spectra for EUVE J0720−317 are consistent with parameters derived from Balmer line spectroscopic fits. The effective temperature and helium abundance for EUVE J2013+400 are consistent with optical spectral analyses; however, the surface gravity is significantly higher than the values determined from Balmer line spectral fits. This higher surface gravity, which corresponds

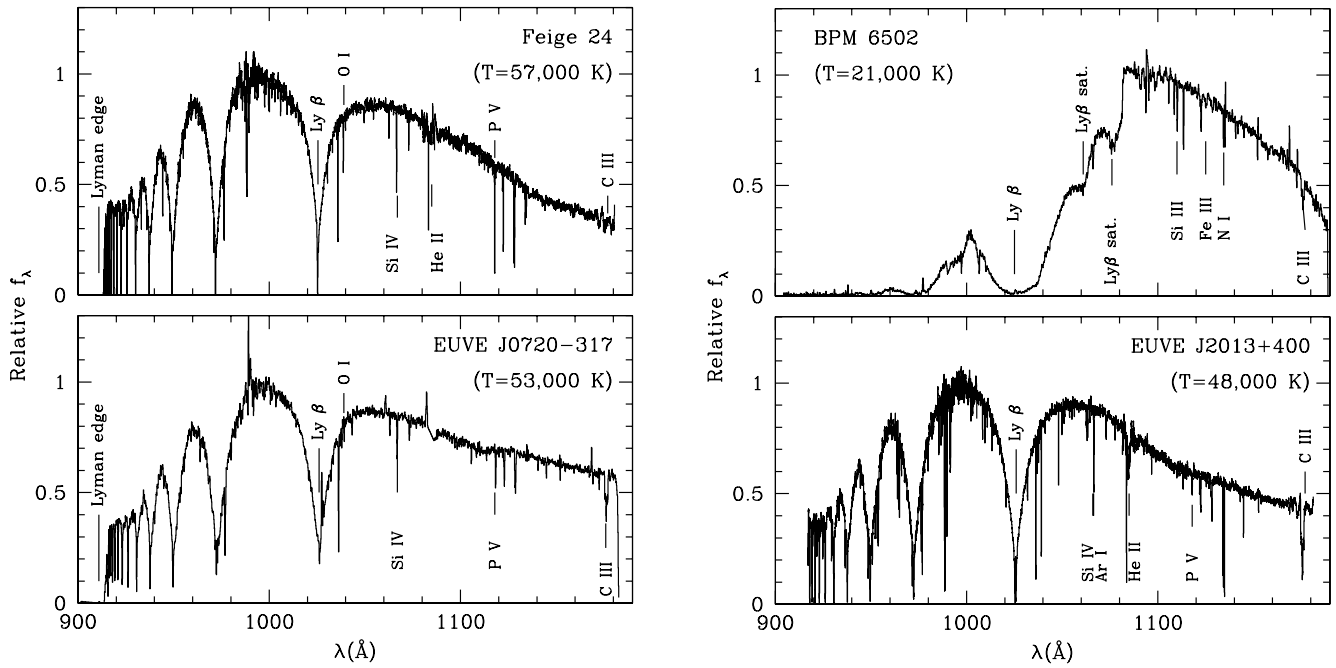

FIG. 1.—*FUSE* spectra of Feige 24, EUVE J0720−317, BPM 6502, and EUVE J2013+400, showing the key heavy elements and ISM lines. [*See the electronic edition of the Journal for a color version of this figure.*]

TABLE 2
PHOTOSPHERIC LINES IN FEIGE 24, J0720−317, AND J2013+400

Ion	λ (Å)	Ion	λ (Å)
N IV	921.994	He II	1084.94[a]
N IV	922.519	Si III	1108.358
N IV	923.676	Si III	1109.97[b]
N IV	924.284	Si III	1113.23[c]
S VI	933.378	P V	1117.978
S VI	944.523	P IV	1118.552[d]
P IV	950.657[c]	S V	1122.042
N IV	955.334	Si IV	1122.485
C III	977.020	P V	128.008
P IV	1030.515[c]	Si IV	1128.34[e]
O VI	1031.912	S V	1128.667
P IV	1033.112[c]	C III	1174.993
P IV	1035.516[c]	C III	1175.263
O VI	1037.613	C III	1175.590
S IV	1062.664	C III	1175.711
S IV	1066.63[f]	C III	1175.987
S IV	1072.973	C III	1176.370
S IV	1073.518		

[a] In Feige 24 only. P IV 950.657 may be blended with ISM O I 950.885.
[b] Blend of 1066.614, 1066.636 and 1066.650 Å.
[c] In J0720−317 and J2013+400 only.
[d] Blend of 1109.940 and 1109.970 Å.
[e] Blend of 1113.174, 1113.204 and 1113.230 Å.
[f] Blend of 1128.325 and 1128.340 Å.

TABLE 3
PHOTOSPHERIC LINES IN BPM 6502

Ion	λ (Å)
N II	1083.990
N II	1084.576[a]
N II	1085.545[b]
N II	1085.701
Si III	1108.358
Si III	1109.97[c]
Si III	1113.23[d]
Si IV	1122.485
Fe III	1122.526
Fe III	1124.881
Fe III	1126.729
Fe III	1128.050
Si IV	1128.34[e]
Fe III	1128.724
Fe III	1129.191
C III	1174.933
C III	1175.263
C III	1175.590
C III	1175.711
C III	1175.987
C III	1176.370

[a] Blend of 1084.562 and 1084.580 Å.
[b] Blend of 1085.529 and 1085.546 Å.
[c] Blend of 1109.940 and 1109.970 Å.
[d] Blend of 1113.174, 1113.204, and 1113.230 Å.
[e] Blend of 1128.325 and 1128.340 Å.

to a mass of $0.80 \pm 0.02\,M_{\odot}$ (using the mass-radius relations of Wood 1995), is also significantly higher than the mass ($0.64 \pm 0.03\,M_{\odot}$) determined from the gravitational redshift of Vennes et al. (1999). We adopt the optical values in this work until this discrepancy is resolved. We discuss this problem further in § 4.4.

Table 4 summarizes the atmospheric properties of the white dwarfs determined from *FUSE* spectra. The table also compares these white dwarf parameters to the same parameters based on optical spectroscopic studies.

4. BINARY PARAMETERS

We used the *FUSE* spectra to obtain radial velocities of the four white dwarfs in the binary systems Feige 24, EUVE J0720−317, BPM 6502, and EUVE J2013+400. These new radial velocity measurements are given in Table 5. We phased the white dwarf radial velocities using published binary ephemerides and determined the velocity semiamplitude $K_{\rm WD}$ and mean velocity $\gamma_{\rm WD}$. These new parameters are then combined with the results of previous optical studies of the red dwarf companions, which listed the red dwarf velocity semiamplitudes ($K_{\rm RD}$) and mean velocities ($\gamma_{\rm RD}$). From this set of measurements we calculated the binary mass ratios and the white dwarf gravitational redshifts ($v_{g,\rm WD}$) for all four systems. Figure 2 shows the radial velocity measurements of the four binaries folded on their orbital period.

Two small corrections were applied to the red dwarf data. First, a determination of the systemic velocity $\gamma_{\rm sys}$ requires that we subtract an estimate of the gravitational redshift of the red dwarf ($v_{g,\rm RD}$) from its mean velocity. Second, a correction is applied to the red dwarf velocity semiamplitude to take into account the nonuniform distribution of the Hα emission over the red dwarf surface. Both corrections require initial estimates of the red dwarf mass and radius. These estimates could be obtained by adopting a mass and radius corresponding to published companion spectral type, but we favor the following approach.

The strength of the Hα emission line has been observed to vary in all four systems (Vennes & Thorstensen 1994b; Kawka et al. 2002; Thorstensen et al. 1994) and is maximum near superior conjunction. These cyclical variations are explained by the changing viewing angle of the irradiated red dwarf hemisphere over the binary period (Thorstensen et al. 1978). In these systems, the Hα emission originates from the irradiated hemisphere and traces an orbit that is lower than the true center-of-mass orbit. The irradiating flux originates from the hot photosphere of the white dwarf (e.g., Feige 24), or, alternatively, from a hypothetical hot accretion region on the surface of the white dwarf, as proposed by Maxted et al. (1998) in the case of GD 448.

We correct for the irradiation effect using the formalism described by Vennes et al. (1999). Wade & Horne (1988) and Orosz et al. (1999) discuss a calculation assuming an irradiated hemisphere that employs the same formalism. The correction term uses a preliminary estimate of the red dwarf radius obtained using a spectroscopic determination of the white dwarf mass and the uncorrected mass ratio. The red dwarf radius is then calculated using the mass-radius relations of Caillault & Patterson (1990). The procedure may be iterated at will. However, the initial correction to the mass ratio being of the order of a few percent (5% to 8%), further iterations are futile.

Final estimates of the red dwarf mass and radius are calculated from the corrected mass ratio and the mass of the white dwarf and from the mass-radius relations of Caillault & Patterson (1990). Next, the gravitational redshift of the red dwarf is calculated using $v_g = 0.63608 M(M_{\odot})/R(R_{\odot})$ km s^{-1} and is typically of the order of 0.5 km s^{-1}. Finally, the systemic velocity is calculated using $\gamma_{\rm sys} = \gamma_{\rm RD} - v_{g,\rm RD}$. Recent measurements of late-type main-sequence stars using interferometry and eclipsing

TABLE 4
PROPERTIES OF THE WHITE DWARF AND ITS COOL COMPANION

Parameter[a]	Feige 24	EUVE J0720−317	BPM 6502	EUVE J2013+400
White Dwarf				
$T_{\rm eff,opt}$ (K)	57,000 ± 2000[b]	52,400 ± 1800[c]	19,960 ± 400[d]	48,000 ± 900[e]
$T_{\rm eff,\,FUSE}$ (K)	[f]	52,750 ± 150	[g]	47,800 ± 200
log $g_{\rm opt}$ (cgs)	7.66 ± 0.08	7.68 ± 0.01[c]	7.86 ± 0.09[d]	7.69 ± 0.09[e]
log g_{FUSE} (cgs	[f]	7.73 ± 0.02	[g]	8.20 ± 0.03
log ($N_{\rm He}/N_{\rm H}$)	...	−3.28 ± 0.08	...	−2.90 ± 0.08
$M_{\rm opt}$ ($M_\odot$)	0.58 ± 0.05[h]	0.56 ± 0.04[c]	0.55 ± 0.05	0.56 ± 0.03[e]
v_g (km s^{-1})	20.1 ± 1.9	21.4 ± 1.9	17.9 ± 0.5	34.0 ± 1.3
$M_{\rm GR}$ ($M_\odot$)	0.57 ± 0.03	0.58 ± 0.03	0.46 ± 0.01	0.71 ± 0.02
Red Dwarf				
M ($M_\odot$)	0.39 ± 0.02	0.43 ± 0.03	0.14 ± 0.01	0.23 ± 0.01
R ($R_\odot$)	0.43 ± 0.02	0.47 ± 0.03	0.19 ± 0.02	0.29 ± 0.01
v_g (km s^{-1})	0.6 ± 0.1	0.6 ± 0.1	0.5 ± 0.1	0.5 ± 0.1
Spectral type	M2	M2	M5	M3

[a] All parameters are determined in this work unless indicated otherwise.
[b] From Vennes & Lanz (2001).
[c] From Vennes et al. (1997a).
[d] From Kawka et al. (2007).
[e] From Vennes et al. (1999).
[f] See text.
[g] See Hébrard et al. (2003) for a comparison between optical parameters and *FUSE* spectrophotometry (see text for details).
[h] Determined using the measured parallax.

binaries show a relatively large scatter in the mass-radius relations for these stars (Berger et al. 2006; López-Morales 2007). Rebassa-Mansergas et al. (2007) show that a similar scatter is observed in the late-type main-sequence companions to white dwarf stars. However, the effect of this scatter on the gravitational redshift of the secondary is less than 0.1 km s^{-1} and does not affect our results.

We estimate the spectral type of the secondary stars using the mass-type relations of Kirkpatrick & McCarthy (1994), but we corroborate our spectral type determination using Two Micron All Sky Survey (2MASS) JHK_s photometry. First, we calculate the absolute JHK magnitudes of the white dwarfs. These white dwarf magnitudes are then converted from CIT to 2MASS using Cutri et al. (2006).[6] Next, we calculate the absolute magnitude of the system using the geometric parallax (Feige 24) or an ultraviolet-based photometric parallax of the white dwarf uncontaminated by the companion (EUVE J0720−317, BPM 6502, and EUVE J2013+400). Next, we subtract the white dwarf contribution. Figure 3 shows the 2MASS JHK_s of the secondary companions in the binary systems, Feige 24, EUVE J0720−317, BPM 6502, and EUVE J2013+400, compared to the colors for cool main-sequence stars (Bessell & Brett 1988; Bessell 1991) converted to 2MASS using Cutri et al. (2006).

Finally, we determine the gravitational redshift of the white dwarf (v_g) by subtracting the systemic velocity ($\gamma_{\rm sys}$) from the white dwarf mean velocity ($\gamma_{\rm WD}$). Then, we convert the gravitational redshift of the white dwarf into a mass estimate using the mass-radius relations of Wood (1995).

With this general frame of work in mind, we now discuss each system separately. The binary properties of these systems are given in Table 6, while the properties of the component stars are given in Table 4.

[6] Available at http://www.ipac.caltech.edu/2mass/releases/allsky/doc/explsup.html.

4.1. *Feige 24*

Thorstensen et al. (1978) were the first to obtain orbital parameters for Feige 24 by measuring the red dwarf radial velocities using Hα and He I emission lines. Vennes & Thorstensen (1994b) determined an orbital period of 4.23160 ± 0.00002 days, and by using the absorption lines they measured a red dwarf velocity semiamplitude of 75.5 ± 2.1 km s^{-1}, with a red dwarf mean velocity of $\gamma_{\rm RD}$ = 62.0 ± 1.4 km s^{-1}. Therefore, the measurements represent the true orbit traced by the secondary center of mass.

Vennes et al. (2000) obtained *Hubble Space Telescope* (*HST*) STIS spectra at orbital quadratures and obtained an estimate of the white dwarf semiamplitude of 49.1 ± 0.3 km s^{-1} and a white dwarf mean velocity of 79.6 ± 2.3 km s^{-1}. We measured the radial velocities of the white dwarf using the Si IV λ1066.63 line in the *FUSE* spectra. We used the interstellar medium (ISM) line of O I λ1039.230 to fix the zero point of the wavelength calibration. We fixed the velocity of the ISM to +7.4 km s^{-1}, which is the mean velocity of the two ISM components in the line of sight of Feige 24 (Vennes et al. 2000). We phased the *FUSE* data to the orbital ephemeris of Vennes & Thorstensen (1994b) to obtain a white dwarf semiamplitude of 51.2 ± 0.6 km s^{-1}, with a white dwarf mean velocity of 81.6 ± 0.4 km s^{-1}. The *FUSE* and *HST* white dwarf mean velocities are in agreement within uncertainties; however, the white dwarf semiamplitude determined using *FUSE* is slightly larger than determined by *HST*. Note that the *FUSE* spectra lacks coverage at one of the quadratures (Φ = 0.25). Combining the *FUSE* and *HST* data, we obtain $K_{\rm WD}$ = 51.0 ± 0.5 km s^{-1} and $\gamma_{\rm WD}$ = 81.5 ± 0.4 km s^{-1}. Figure 2 shows the radial velocity measurements folded on the orbital period.

A minimum white dwarf mass of 0.53 $M_\odot$ is obtained using Kepler's third law. Vennes et al. (2000) estimated a white dwarf mass of 0.55 ± 0.02 $M_\odot$ using the parallax measurement of

TABLE 5
FUSE Radial Velocity Measurements

HJD (2,450,000+)	Phase	v (km s^{-1})	HJD (2,450,000+)	Phase	v (km s^{-1})	HJD (2,450,000+)	Phase	v (km s^{-1})
			Feige 24					
2,980.556641	0.306	39.09	3,007.908447	0.770	134.65	3,010.681641	0.425	61.57
2,980.738525	0.349	40.54	3,007.925049	0.774	133.33	3010.697021	0.429	56.18
2,980.743408	0.350	40.18	3,007.987061	0.788	136.60	3,010.749023	0.441	58.40
2,980.760498	0.354	43.99	3,008.000000	0.792	133.43	3,010.768555	0.446	67.56
2,980.765381	0.355	44.90	3,008.049072	0.803	130.67	3,010.820312	0.458	67.60
3,007.428223	0.656	122.77	3,008.063721	0.807	130.21	3,010.837158	0.462	68.66
3,007.443359	0.660	126.06	3,008.118164	0.819	128.69	3,010.905273	0.478	74.85
3,007.492432	0.672	127.64	3,008.133545	0.823	129.36	3,010.964844	0.492	76.92
3,007.509277	0.676	124.60	3,008.188477	0.836	123.89	3,010.980957	0.496	76.64
3,007.562744	0.688	125.24	3,008.271729	0.856	126.05	3,011.031006	0.508	78.30
3,007.578125	0.692	129.65	3,008.325439	0.868	119.41	3,011.044678	0.511	83.00
3,007.631592	0.704	127.55	3,008.341064	0.872	119.50	3,011.097412	0.523	90.51
3,007.706787	0.722	132.29	3,008.394775	0.885	116.56	3,011.118652	0.528	90.47
3,007.769775	0.737	133.51	3,008.410400	0.889	117.65	3,011.167725	0.540	92.46
3,007.786621	0.741	130.78	3,008.462891	0.901	109.57	3,011.183594	0.544	93.12
3,007.839355	0.754	133.54	3,010.547607	0.393	46.78	3,011.238281	0.557	97.22
3,007.855713	0.757	131.35	3,010.613037	0.409	54.23	3,011.251465	0.560	99.58
			EUVE J0720−317					
2,226.887805	0.682	125.4	2,227.024896	0.791	127.5	2,227.164429	0.902	93.7
2,226.954556	0.735	129.5	2,227.095490	0.847	112.2	...	...	...
			BPM 6502					
2,452.329834	0.742	43.94	2,452.636963	0.654	40.07	3,758.507324	0.115	12.14
2,452.383789	0.902	37.55	2,452.708984	0.868	39.26	4,161.851074	0.745	46.36
2,452.438965	0.066	17.22	3,757.399658	0.826	42.38	4,161.914062	0.933	35.11
2,452.491455	0.222	6.87	3,757.468994	0.032	23.22	4,161.984863	0.143	13.60
2,452.562256	0.432	17.30	3,758.439453	0.914	35.99	4,162.055664	0.353	12.88
			EUVE J2013+400					
1,858.616821	0.261	−31.31	2,934.230957	0.833	31.12	2935.272705	0.309	−31.28
1,858.688843	0.363	−25.97	2,934.303467	0.935	16.50	2935.344727	0.412	−18.91
1,858.759399	0.463	2.42	2,934.374268	0.036	−7.95	2,935.411865	0.506	12.85
1,858.827881	0.560	11.69	2,934.441895	0.132	−25.66	2935.453857	0.566	21.00
2,576.795898	0.206	−28.09	2,934.483887	0.191	−32.40	2,935.482422	0.606	30.27
2,576.863037	0.301	−25.85	2,934.512695	0.232	−27.90	2935.526123	0.668	33.93
2,576.932129	0.399	−9.26	2,934.557617	0.296	−32.68	2,935.553223	0.707	36.46
2,577.002197	0.498	12.66	2,934.631348	0.400	−15.26	2,935.599121	0.772	40.11
2,577.075684	0.603	34.30	2,934.712891	0.516	22.12	2,935.622559	0.805	35.33
2,936.028809	0.381	−21.45	2,934.767090	0.593	24.37	2,935.672607	0.876	28.87
2,936.099121	0.481	3.57	2,934.782471	0.614	29.15	2,935.689697	0.900	23.53
2,936.169678	0.581	29.15	2,934.834961	0.689	37.86	2,935.736572	0.967	14.54
2,936.241455	0.682	35.89	2,934.851807	0.712	40.96	2,935.805664	0.065	−16.10
2,936.312500	0.783	35.89	2,934.904785	0.788	40.11	2,935.822266	0.088	−21.72
2,936.383301	0.884	22.68	2,934.920898	0.811	36.46	2,935.875000	0.163	−25.94
2,934.023438	0.539	21.84	2,934.987793	0.906	23.53	2,935.891602	0.187	−31.84
2,934.082764	0.623	37.02	2,935.065674	0.016	−12.73	2,935.946045	0.264	−32.96
2,934.096191	0.642	34.77	2,935.125244	0.100	−23.97	2,935.960938	0.285	−32.40
2,934.156982	0.728	37.30	2,935.137695	0.118	−25.38			
2,934.167969	0.744	40.11	2,935.199219	0.205	−32.96			

$\pi = 14.7 \pm 0.6$ mas (Benedict et al. 2000) and $V = 12.56 \pm 0.05$ for the white dwarf (Holberg et al. 1986), adopting $T_{\rm eff} = 56{,}000 \pm 1000$ K. Using an effective temperature of $57{,}000 \pm 2000$ K, we obtain a mass of $0.58 \pm 0.05\ M_{\odot}$. Note that the increased error in the temperature results in an increased error in the mass determination.

We determined the white dwarf gravitational redshift to be $v_g = 20.1 \pm 1.9$ km s^{-1}. The gravitational redshift of the red dwarf was assumed to be 0.6 ± 0.1 km s^{-1} (see below). The gravitational redshift of the white dwarf corresponds to a mass of $0.57 \pm 0.03\ M_{\odot}$.

Since the two mass estimates agree, we adopt a mass of $0.57 \pm 0.03\ M_{\odot}$ for the white dwarf, which is the weighted mean of the two mass determinations discussed above. The corresponding surface gravity would be $\log g = 7.66 \pm 0.08$. The mass ratio of the system is $q = K_{\rm WD}/K_{\rm RD} = M_{\rm RD}/M_{\rm WD} = 0.68$,

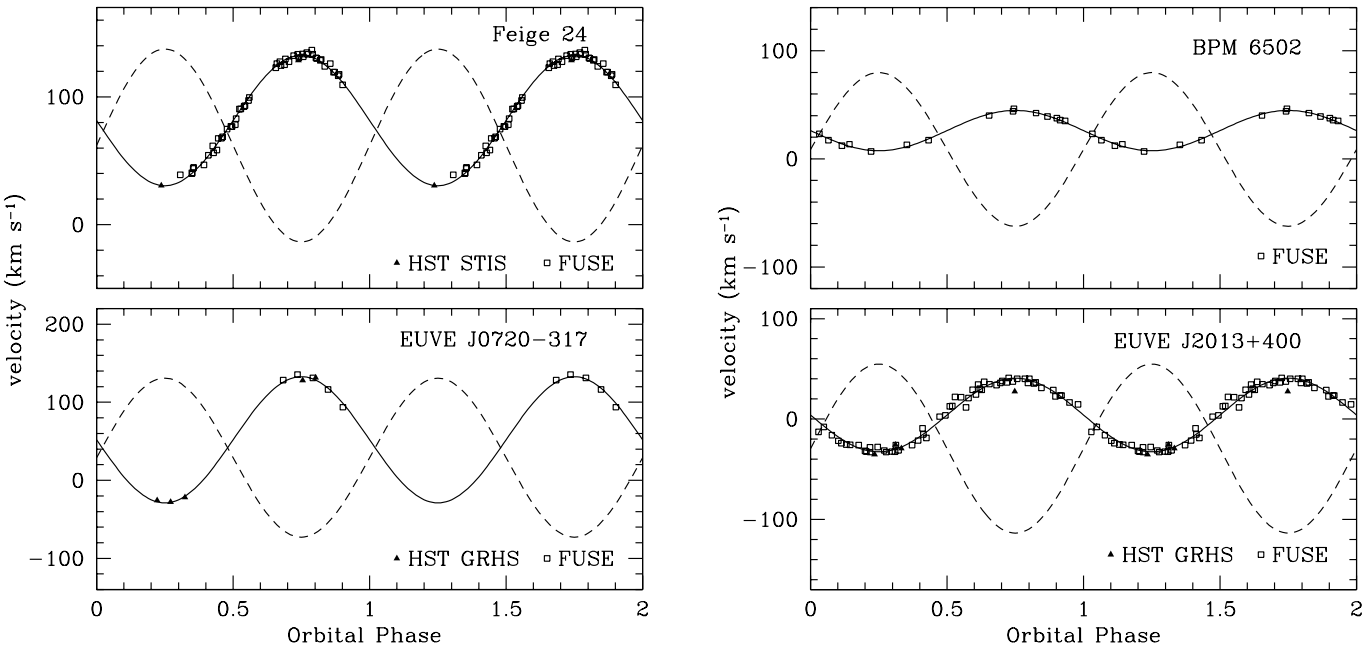

FIG. 2.—Radial velocities of the white dwarf in Feige 24, EUVE J0720−317, BPM 6502, and EUVE J2013+400, folded on the orbital period as described in the text.

which results in a mass of $0.39 \pm 0.02\ M_\odot$ for the secondary. With a radius of $0.43 \pm 0.02\ R_\odot$, we obtain a gravitational redshift of 0.6 ± 0.1 km s^{-1}. The mass function of $f(M_{\rm WD}) = 0.189 \pm 0.016$ implies that the inclination of the system is $i = 77.4^\circ \pm 3.5^\circ$.

The derived mass ($0.39\ M_\odot$) translates to a spectral type of dM1.5-2 for the secondary star. Using the 2MASS photometry of the binary system ($J = 11.265 \pm 0.024$, $H = 10.733 \pm 0.022$, and $K_s = 10.557 \pm 0.019$), we calculated the absolute magnitudes of the secondary, $M_J = 7.28$, $M_H = 6.65$, and $M_K = 6.45$. In our calculations we used the parallax distance of 68.4 ± 2.0 pc (Benedict et al. 2000). Figure 3 shows that the spectral type of the secondary based on 2MASS colors ($J - H = 0.63$ and $H - K_s = 0.20$) ranges from ~K6 to M2.

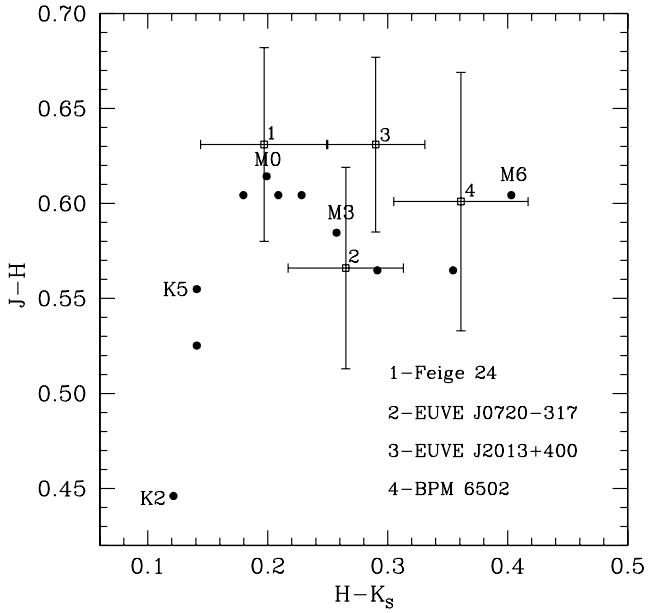

FIG. 3.—2MASS $J - H$ vs. $H - K_s$ color diagram showing the colors of the secondary stars (corrected for the white dwarf contribution) in Feige 24, EUVE J0720−317, EUVE J2013+400, and BPM 6502 (*squares*), compared to main-sequence colors (*circles*).

The binary parameters and mass of the secondary ($0.39\ M_\odot$) suggest that magnetic braking will be the main angular momentum loss for the system, and using the equations from Schreiber & Gänsicke (2003) and Ritter (1986), we find that the secondary star will fill its Roche lobe and begin mass transfer with a period of 0.164 days in $\sim 2.2 \times 10^{11}$ yr. Therefore, Feige 24 is not representative of the progenitors of the current population of cataclysmic variables.

4.2. *EUVE J0720−317*

EUVE J0720−317 was identified as a post-CE binary by Vennes & Thorstensen (1994a). Kawka et al. (2002) measured an orbital period for the binary of 1.262396 ± 0.000008 days and a velocity semiamplitude of the red dwarf of 98.2 ± 1.2 km s^{-1}, with a red dwarf mean velocity of $\gamma_{\rm RD} = 31.1 \pm 0.7$ km s^{-1}. Vennes et al. (1999) used *HST* spectra to trace the orbit of the white dwarf and measured the white dwarf semiamplitude to be 79.5 ± 1.4 km s^{-1}. We have measured the radial velocities of the white dwarf using the Si IV λ1066.63 line in the *FUSE* spectra. We used the ISM line of O I λ1039.230 to fix the zero point of the wavelength calibration. The velocity of the local interstellar cloud (LIC) in the direction of EUVE J0720−317 is 13.5 km s^{-1} (Lallement et al. 1995); however, the measured velocity of O I λ1039.230 is 6.7 km s^{-1}. Therefore, all measured velocities were shifted by +6.8 km s^{-1}. Combining the *FUSE* velocity measurements with the *HST* velocities, we updated the white dwarf semiamplitude to $K_{\rm WD} = 80.8 \pm 1.2$ km s^{-1} and $\gamma_{\rm WD} = 51.9 \pm 1.1$ km s^{-1}. Figure 2 shows the radial velocities of the white dwarf folded on the orbital period.

We corrected the red dwarf semiamplitude to obtain 105.9 ± 3.4 km s^{-1}, from which we estimate a mass ratio of $q = 0.76 \pm 0.03$. Using the white dwarf mass of $0.56 \pm 0.04\ M_\odot$ from Vennes et al. (1997b) and our measured mass ratio, we estimate the mass for the red dwarf to be $M_{\rm RD} = 0.43 \pm 0.03\ M_\odot$, with a radius of $0.47 \pm 0.03\ R_\odot$. Adopting the corrected mass function of $f(M_{\rm WD}) = 0.155 \pm 0.015\ M_\odot$, we find the inclination of the system to be $i = 72.2^\circ \pm 1.8^\circ$.

TABLE 6
Binary Parameters

Parameter	Feige 24	EUVE J0720−317	BPM 6502	EUVE J2013+400
m_V	12.4	14.0	13.0	14.8
Period (days)	4.23160 ± 0.00002[a]	1.262396 ± 0.000008[b]	0.3367849 ± 0.0000006	0.705517 ± 0.000006[c]
K_{RD} (km s^{-1})	75.5 ± 2.1[a,d]	98.2 ± 1.2[b]	71.1 ± 0.2	84.2 ± 0.9[c]
$K_{RD,corr}$ (km s^{-1})	...	105.9 ± 3.4	75.2 ± 3.1	89.1 ± 2.6
γ_{RD} (km s^{-1})	62.0 ± 1.4[a]	31.1 ± 0.7[b]	8.7 ± 0.1	−29.5 ± 0.7[c]
γ_{sys} (km s^{-1})	61.4 ± 1.5	30.5 ± 0.8	8.2 ± 0.2	−30.0 ± 0.8
K_{WD} (km s^{-1})	51.0 ± 0.5	80.8 ± 1.2	18.6 ± 0.5	36.7 ± 0.7
γ_{WD} (km s^{-1})	81.5 ± 0.4	51.9 ± 1.1	26.1 ± 0.3	4.0 ± 0.5
q	0.68 ± 0.02	0.76 ± 0.03	0.25 ± 0.01	0.41 ± 0.01
i (deg)	77.4 ± 3.5	72.2 ± 1.8	20.3 ± 0.3	34.7 ± 0.5
$f(m\mathrm{WD})$ ($M_\odot$)	0.189 ± 0.016	0.155 ± 0.015	0.015 ± 0.002	0.052 ± 0.005

[a] From Vennes & Thorstensen (1994b).
[b] From Kawka et al. (2002).
[c] From Vennes et al. (1999).
[d] Based on red dwarf absorption velocities.

The derived mass translates to a spectral type of dM1-2 for the secondary star. Using the 2MASS photometry of the binary system ($J = 13.253 \pm 0.025$, $H = 12.749 \pm 0.026$, and $K_s = 12.502 \pm 0.027$), we calculated the absolute magnitudes of the secondary to be $M_J = 6.95$, $M_H = 6.38$, and $M_K = 6.12$. To estimate the distance toward EUVE J0720−317, we obtained short-wavelength *International Ultraviolet Explorer* (*IUE*) spectra (SWP 54496 and 54497) and compared them to a synthetic spectrum with the white dwarf parameters ($T_{\rm eff} = 52,400$ K and $\log g = 7.68$). The distance (d) to EUVE J0720−317 would then be when the difference between the observed spectrum and the model spectrum (F) placed at given distance, i.e., $(R/d)^2F$ is minimized. The radius of the white dwarf (R) is calculated using the mass-radius relations of Wood (1995). Figure 3 shows that the spectral type of the secondary based on 2MASS colors ($J - H = 0.56$ and $H - K_s = 0.26$) is ∼dM3.

We determined the white dwarf gravitational redshift to be $v_g = 21.4 \pm 1.9$ km s^{-1}. A red dwarf gravitational redshift of 0.6 ± 0.1 km s^{-1} was used. The gravitational redshift of the white dwarf corresponds to a mass of $0.58 \pm 0.03\ M_\odot$, which is in agreement with the mass determined from a spectroscopic fit of the Balmer lines (Table 6).

The binary parameters and the relatively large secondary mass suggest that magnetic braking will be the main angular momentum loss for the system, and using the equations from Schreiber & Gänsicke (2003) and Ritter (1986), we conclude that the secondary star will fill its Roche lobe and begin mass transfer with a period of 0.175 days (4.21 hr) in $\sim 3.2 \times 10^9$ yr. The contact period of 3.31 hr reported by Vennes et al. (1999) is shorter than the one we determined in this work, because of a larger secondary mass and hence higher mass ratio than the values used in Vennes et al. (1999). Due to the large mass ratio, dynamically unstable mass transfer will be initiated when the system comes into contact (de Kool 1992).

4.3. *BPM 6502*

4.3.1. *Orbital Period*

BPM 6502 was identified as a post-CE binary by Kawka et al. (2000). Kawka et al. (2002) measured an orbital period of 0.336784 ± 0.000001 days; however, Morales-Rueda et al. (2005) report a period of 0.337083 ± 0.000001 days, which is significantly longer. The period determined by Kawka et al. (2002) corresponds to their third alias. We have reanalyzed these two data sets, and we show that the correct orbital period of BPM 6502 is the one reported by Kawka et al. (2002).

The first step of our analysis was to determine the period of the two sets independently. The orbital period using measurements of Kawka et al. (2002) is 0.336784 ± 0.000001 days, as reported. Aliases in the analysis are observed, but all of them are significantly below the 3 σ confidence level. The top panel of Figure 4 shows the periodogram of these measurements, and the top panel of Figure 5 shows Hα radial velocity measurements from both sets of data folded over the orbital period. Using the radial velocity measurements reported by Morales-Rueda et al. (2005), we reproduced the most probable orbital period of 0.337083 ± 0.000004 days and the several aliases as reported in their analysis. We find that four possible periods are within the 3 σ confidence level, including two that fall within 1 σ. The

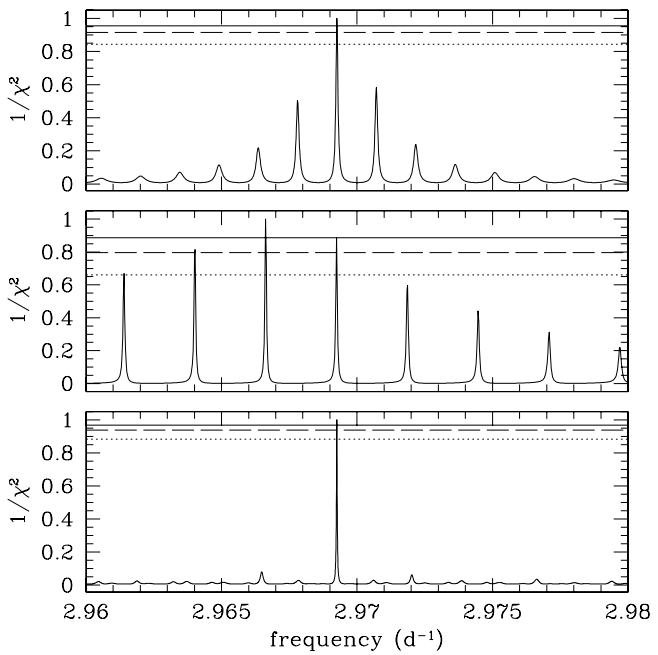

Fig. 4.— *Top*: Periodogram of the radial velocities measured by Kawka et al. (2002). *Middle*: Periodogram of the radial velocities measured by Morales-Rueda et al. (2005). *Bottom*: Periodogram of the combined radial velocities. The lines show the 1 σ (*solid line*), 2 σ (*dashed line*), and 3 σ (*dotted line*) confidence levels.

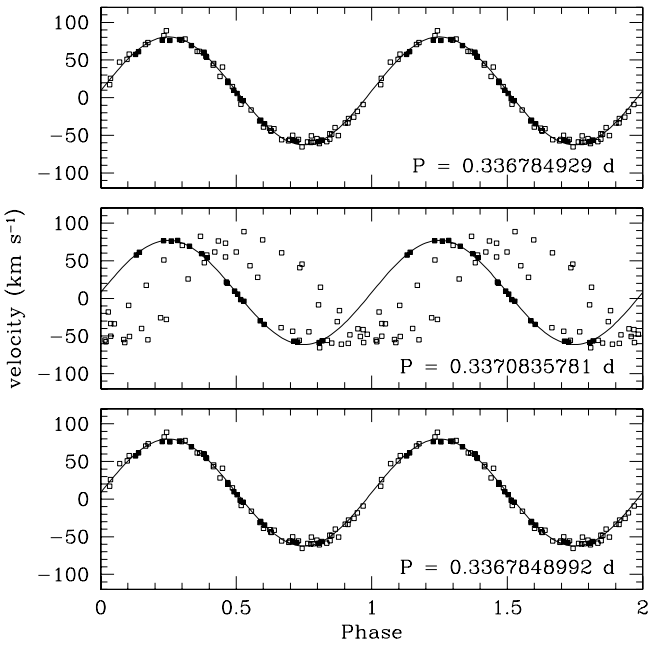

FIG. 5.—Radial velocities of the red dwarf in BPM 6502 traced by Hα and folded on the orbital period, as determined by Kawka et al. (2002; *top*) and Morales-Rueda et al. (2005; *middle*), and the period determined by combining the radial velocity measurements from both studies (*bottom*). Velocities measured by Kawka et al. (2002) are indicated by open squares, and velocities measured by Morales-Rueda et al. (2005) are indicated by filled squares.

second peak that falls within 1 σ corresponds to a period of 0.336786 days, which corresponds to the period determined by Kawka et al. (2002). Therefore, using the data of Morales-Rueda et al. (2005) alone, the remaining three aliases cannot be excluded as possible orbital periods of the system. The middle panel of Figure 4 shows the periodogram of these measurements, clearly showing that the other aliases cannot be excluded. The middle panel of Figure 5 shows Hα radial velocity measurements from both sets of data folded over the best orbital period. Here the measurements taken during HJD 2,451,0143–HJD 2,451,0528 (Morales-Rueda et al. 2005) follow the calculated orbital velocities; however, the measurements taken almost 3 years later (HJD 2,451,607–HJD 2,451,634; Kawka et al. 2000) and a further 2 years later (HJD 2,452,301–HJD 2,452,317; Kawka et al. 2002) are out of phase.

Using both sets of data, we found that the best orbital period is

$$P = 0.3367849 \pm 0.0000006 \text{ days},$$

and the epoch of inferior conjunction is

$$T_0 = 2,450,143.4195 \pm 0.0003,$$

where the new ephemeris is formally in agreement with Kawka et al. (2002). The bottom panel of Figure 4 shows the periodogram of these measurements, where the aliases have almost disappeared. The bottom panel of Figure 5 shows Hα radial velocity measurements from both sets of data folded over the best orbital period. The semiamplitude of the combined measurements is $K_{\rm WD} = 71.1 \pm 0.2$ km s^{-1}, with a red dwarf mean velocity, $\gamma_{\rm RD} = 8.7 \pm 0.1$ km s^{-1}.

4.3.2. *White Dwarf Radial Velocity Measurements*

We measured the radial velocities of the white dwarf using the narrow Si III lines $\lambda\lambda$1108.358, 1109.962, and 1113.225 in *FUSE* spectra. We used the ISM lines of N I $\lambda\lambda$1134.165, 1134.415, and 1134.980 to fix the zero point of the wavelength calibration. All sets of velocity measurements were corrected such that the ISM velocity is equal to $v_{\rm ISM} = -7$ km s^{-1} (Lallement et al. 1995). The semiamplitude of the white dwarf radial velocity measurements is $K_{\rm WD} = 18.6 \pm 0.5$ km s^{-1} and $\gamma_{\rm WD} = 26.1 \pm 0.3$ km s^{-1}. Figure 2 shows the radial velocities of the white dwarf folded over the period.

The Hα emission in BPM 6502 is assumed to have originated from the irradiated hemisphere of the red dwarf (Kawka et al. 2002), and therefore we corrected the red dwarf semiamplitude to 75.2 ± 3.1 km s^{-1}. Using the corrected red dwarf semiamplitude, we estimate a mass ratio of $q = 0.25 \pm 0.01$. The white dwarf mass of $0.55 \pm 0.05\,M_\odot$ was estimated from Kawka et al. (2007) using the mass-radius relations of Wood (1995). From our measured mass ratio, we estimate the mass for the red dwarf to be $M_{\rm RD} = 0.14 \pm 0.01\,M_\odot$, with a radius of $0.19 \pm 0.02\,R_\odot$. Adopting the corrected mass function of $f(M_{\rm WD}) = 0.015 \pm 0.002\,M_\odot$, we find the inclination of the system to be $i = 20.3^\circ \pm 0.3^\circ$.

The derived mass ($0.14\,M_\odot$) translates to a spectral type of dM4.5($\pm$0.5). Using 2MASS photometry of BPM 6502 (11.423 ± 0.026, $H = 10.896 \pm 0.027$, and $K_s = 10.561 \pm 0.021$), we calculated the absolute magnitudes of the secondary, $M_J = 8.88$, $M_H = 8.29$, and $M_K = 7.93$. We determined the distance of BPM 6502 using *IUE* spectra (SWP 27351) in the same way as for EUVE J0720−317. Figure 3 shows that the spectral type of the secondary based on 2MASS colors ($J - H = 0.60$ and $H - K = 0.36$) is ~dM5. Tappert et al. (2007) obtained *K*-band spectroscopy, for which the spectral energy distribution suggests a spectral type ranging from M2.5 to M5, but the Na I and Ca I line strengths favor a latter spectral type of M5. Taking into account all the available data, we adopt a spectral type of dM5.

We determined the white dwarf gravitational redshift to be $v_g = 17.9 \pm 0.5$ km s^{-1}, which corresponds to a mass of $0.46 \pm 0.01\,M_\odot$. A red dwarf gravitational redshift of $v_g = 0.5 \pm 0.1$ km s^{-1} was used. This mass is significantly different from the spectroscopic mass of $0.55 \pm 0.05\,M_\odot$. Previous gravitational redshift measurements of the white dwarfs using Balmer lines resulted in much higher values, 42.2 ± 9.0 km s^{-1} (Kawka et al. 2000) and 36.16 ± 2.72 km s^{-1} (Morales-Rueda et al. 2005). It is likely that the Balmer line cores are contaminated by the red dwarf even after the subtraction of the emission line. In the case of using the *FUSE* spectra of the white dwarf to measure the radial velocity, the zero point depends on the adopted ISM velocity. We have assumed that the N I lines originate only from the LIC; however, another cloud in the line of sight toward BPM 6502 could shift the velocity scale. Future high-dispersion ultraviolet observations of the line of sight toward BPM 6502 may well be able to resolve velocity structures in ISM spectral lines and provide a more reliable anchor for ultraviolet line velocities.

The binary parameters and the relatively small secondary mass suggest that the major contribution to angular momentum loss is from the release of gravitational radiation. Using the equations from Ritter (1986), the secondary star will fill its Roche lobe and begin mass transfer with a period of 0.083 days in $\sim 3.0 \times 10^{10}$ yr. The time BPM 6502 comes into contact is much longer than for EUVE J0720−317, because magnetic braking is not invoked, due to the low mass of the secondary.

4.4. *EUVE J2013+400*

EUVE J2013+400 was identified as a post-CE binary by Thorstensen et al. (1994). Vennes et al. (1999) measured an orbital period for the binary of 0.705517 ± 0.000006 days and

TABLE 7
Model Atoms Treated Explicitly

Element	BPM 6502					Feige 24, EUVE J0720−317, and EUVE J2013+400					
	I	II	III	IV	V	I	II	III	IV	V	VI
H[a]	9(1)	...	...	...	...	9(1)	...	...	...	...	...
He[a]	...	...	...	...	...	24	20	...	...	...	...
C[a]	...	22(5)	23(7)	25(4)	...	...	22(5)	23(7)	25(4)	...	...
N[a]	...	26(8)	32(7)	23(8)	...	...	...	32(7)	23(8)	16(6)	...
O[a]	...	...	...	...	...	...	...	...	39(8)	40(6)	20(5)
Si[a]	...	8[b]	30(6)	23(4)	...	...	...	30(6)	23(4)	...	...
P[b]	...	...	...	...	...	...	...	...	14	17(4)	...
S[b]	...	...	...	...	...	...	...	...	15	12	16
Fe[a]	...	(36)[c]	(50)	(43)	(42)	...	...	...	(43)	(42)	(32)

[a] OSTAR2002, Lanz & Hubeny (2003).
[b] Earlier version.
[c] BSTAR2006; Lanz & Hubeny (2007).

a semiamplitude for the red dwarf of 84.2 ± 0.9 km s^{-1}, with a mean velocity of $\gamma_{RD} = -29.5 \pm 0.7$ km s^{-1}. Using *HST* spectra, they were able to trace the orbit of the white dwarf, and they measured the white dwarf semiamplitude to be 29.9 ± 2.5 km s^{-1}. We have measured the radial velocities of the white dwarf using the Si IV λ1066.63 line in the *FUSE* spectra. This line is near the ISM line of Ar I λ1066.660, and blends with the Si IV λ1066.63 line for a short duration near orbital conjunction. We included the velocity measurements only when the Si IV and Ar I are clearly separated. Ar I λ1066.660 was used to fix the zero point of the wavelength calibration. Its proximity minimizes the distortion in the wavelength scale due to thermal effects. All sets of velocity measurements were corrected such that the ISM velocity is equal to $v_{ISM} = -8$ km s^{-1} (Lallement et al. 1995). Combining the *FUSE* velocity measurements with the *HST* velocities, we obtain an updated white dwarf semiamplitude of $K_{WD} = 36.7 \pm 0.7$ km s^{-1} and $\gamma_{WD} = 4.0 \pm 0.5$ km s^{-1}. Figure 2 shows the radial velocities of the white dwarf folded over the orbital period.

The Hα emission is assumed to have originated from the irradiated hemisphere of the red dwarf and hence does not trace the motion of the red dwarf center of mass. Therefore, we corrected the red dwarf semiamplitude to 89.1 ± 2.6 km s^{-1}, from which we estimate a mass ratio of $q = 0.41 \pm 0.01$. Using the white dwarf mass of $0.56 \pm 0.03\ M_\odot$ from Vennes et al. (1999) and our measured mass ratio, we estimate the mass for the red dwarf to be $M_{RD} = 0.23 \pm 0.01\ M_\odot$, with a radius of $0.29 \pm 0.01\ R_\odot$. Adopting the corrected mass function of $f(M_{WD}) = 0.052 \pm 0.005\ M_\odot$, we find the inclination of the system to be $i = 34.7^\circ \pm 0.5^\circ$.

The derived mass translates to a spectral type of dM3.5($\pm$0.5) for the secondary star. Using 2MASS photometry of EUVE J2013+400 ($J = 13.044 \pm 0.044$, $H = 12.520 \pm 0.024$, and $K_s = 12.260 \pm 0.032$), we calculated the absolute magnitudes of the secondary to be $M_J = 7.73$, $M_H = 7.09$, and $M_K = 6.80$. We determined the distance of BPM 6502 using *IUE* spectra (SWP 27351) in the same way as for EUVE J0720−317. Figure 3 shows that the spectral type of the secondary based on 2MASS colors ($J - H = 0.64$ and $H - K_s = 0.29$) is $\sim$dM4.

We determined the white dwarf gravitational redshift to be $v_g = 34.0 \pm 1.3$ km s^{-1}, which corresponds to a mass of $0.71 \pm 0.02\ M_\odot$. A red dwarf gravitational redshift of $v_g = 0.5 \pm 0.1$ km s^{-1} was used. This is higher than the mass determined from a spectroscopic fit of the Balmer lines (see Table 6) and higher than the mass of $0.64 \pm 0.03\ M_\odot$ determined from the gravitational redshift by Vennes et al. (1999). Again, as in the case of BPM 6502, the possibility that the adopted LIC velocity is blended with another ISM cloud causing a shift in the velocity scale could explain this difference. Moreover, the mass determined from the *FUSE* spectral fit also indicates a higher mass ($0.80\ M_\odot$). The various mass estimates suggest that the white dwarf mass in EUVE J2013+400 is between 0.56 and $0.80\ M_\odot$.

The binary parameters and the relatively small secondary mass suggest that the major contribution to angular momentum loss is from the release of gravitational radiation. Using the equations from Ritter (1986), the secondary star will fill its Roche lobe and begin mass transfer with a period of 0.118 days in $\sim 1.3 \times 10^{11}$ yr.

5. WHITE DWARF ABUNDANCE ANALYSIS

5.1. *Model Atmospheres*

We computed a series of NLTE model atmospheres using TLUSTY version 200 and SYNSPEC version 48 (Hubeny & Lanz 1995) and adopted stellar parameters for BPM 6502, EUVE J2013+400, EUVE J0720−317, and Feige 24: $T_{eff} = 20{,}000$ K ($\log g = 7.85$), $T_{eff} = 48{,}000$ K ($\log g = 7.7$), $T_{eff} = 52{,}400$ K ($\log g = 7.7$), and $T_{eff} = 57{,}000$ K ($\log g = 7.5$), respectively. Using preliminary abundance estimates, we then bracketed the abundance inputs with models with abundance variations of −0.7, 0, and +0.7 dex. Table 7 summarizes adopted model atoms, including some from Lanz & Hubeny (2003, 2007). The table lists the number of levels included and, between parentheses, the number of superlevels. A superlevel groups together several levels that have close excitation energies and are assumed to be in Boltzmann equilibrium relative to each other. For example, the ion C IV is treated using a total of 25 levels, four of them being superlevels. These four superlevels correspond to the principal quantum number of the external electron $n = 7$, 8, 9, and 10, while detailed configurations are treated explicitly for $n = 2$ (s and p) up to $n = 6$ (s, p, d, f, g, and h). The abundances are then measured using a χ^2 minimization technique applied to observed spectral lines from Tables 2 and 3 and the synthetic spectra.

In the case of EUVE J0720−317 and J2013+400 we also varied the iron abundance between $\log(\mathrm{Fe/H}) = -6$ and −8. The effect on the abundance of lighter elements did not exceed $\pm$0.02 dex. Therefore, we tabulate only abundances obtained with models at $\log(\mathrm{Fe/H}) = -6$. Finally, in the case of Feige 24 we fixed the iron abundance to $\log(\mathrm{Fe/H}) = -5.5$ (Vennes et al. 2000).

TABLE 8
PHOTOSPHERIC ABUNDANCES FOR FEIGE 24, EUVE J0720−317, BPM 6502, AND EUVE J2013+400

	log (X/H)			
ELEMENT	Feige 24	EUVE J0720−317	BPM 6502	EUVE J2013+400
He	...	0.14	$\lesssim -3$	-2.90 ± 0.07
C	-6.90 ± 0.06	-5.75 ± 0.08	-5.68 ± 0.07	-5.50 ± 0.05
N	-6.77 ± 0.10	-6.58 ± 0.17	-6.77 ± 0.21	-5.75 ± 0.14
O	[a]	[a]	...	[a]
Si	-6.20 ± 0.07	-6.27 ± 0.08	-6.93 ± 0.04	-6.38 ± 0.04
P	-7.11 ± 0.05	-7.50 ± 0.10	...	-8.20 ± 0.05
S	-6.36 ± 0.08	-6.71 ± 0.11	...	-6.92 ± 0.05
Fe	(-5.5)[b]	...	-7.32 ± 0.13	...

[a] See text.
[b] Vennes et al. (2000).

We did not attempt vertical variations of the abundance of trace element. Chayer et al. (2003, 2006) show evidence of a stratification of the oxygen abundance in several white dwarfs showing resonance lines of O VI. Vennes & Lanz (2001) also found a discrepancy between abundance measurements based on O IV and O V in Feige 24 and G191 B2B, which could be attributed to a stratification of oxygen in their atmospheres.

5.2. *Analysis*

Table 8 lists the measured abundances in Feige 24, EUVE J0720−317, BPM 6502, and EUVE J2013+400. New *FUSE* abundance measurements in Feige 24 are consistent with the *HST* STIS measurements of Vennes et al. (2000). Figure 6 shows C III line profile fits. The carbon abundance measurements in EUVE J0720−317 and J2013+400 are in agreement with the measurements of Vennes et al. (1999) based on *HST* GHRS spectra of the C IV line profiles. We could not achieve satisfactory fits of the O VI line profiles using the present models. Chayer et al. (2003, 2006) explored the problem in a sample of white dwarfs showing O VI resonance lines and concluded that a reservoir of oxygen concentrated at the top of the atmosphere is able to reproduce the line profiles with a plausible oxygen abundance. We simply note that a similar phenomenon is possibly present in Feige 24, EUVE J0720−317, and EUVE J2013+400, and we exclude the case of oxygen from further consideration.

Figure 7 shows Si IV and Fe III line profile fits in BPM 6502. At $T_{\rm eff} = 20{,}000$ K and $\log({\rm Fe/H}) = -7.3$, BPM 6502 seems to follows a trend noted by Vennes et al. (2006) suggesting a decreasing abundance with decreasing temperatures. However, the abundance of iron in cooler white dwarfs may depend on their immediate environment. For example, the case of GD 362 at $T_{\rm eff} = 9760$ K and $\log({\rm Fe/H}) = -5.5$ (or NLTT 44986; Gianninas et al. 2004; Kawka & Vennes 2006) may reveal the presence of circumstellar debris accreted onto the white dwarf. We could similarly argue that the presence of iron (and of lighter elements) in BPM 6502 is also a signature of accreted material, but from the close late-type companion.

Figure 8 summarizes our new abundance measurements in Feige 24, EUVE J0720−317, BPM 6502, and EUVE J2013+400. The abundance measurements $[({\rm X/H})/({\rm X/H})_{\odot}]$ are normalized to solar values (Asplund et al. 2005) and presented as a function of the atomic number *Z*. Helium is dominant in EUVE

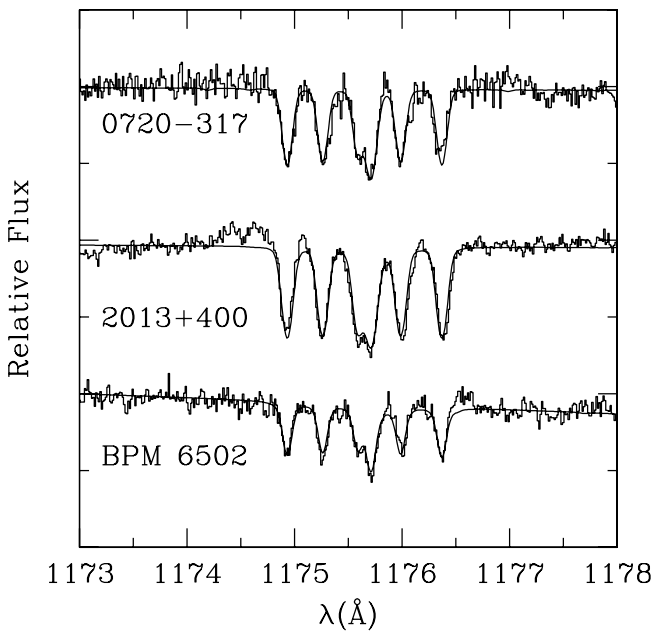

FIG. 6.—*FUSE* spectra showing the C III photospheric lines of EUVE J0720−317, BPM 6502, and EUVE J2013+400 compared to the best-fit models. [*See the electronic edition of the Journal for a color version of this figure.*]

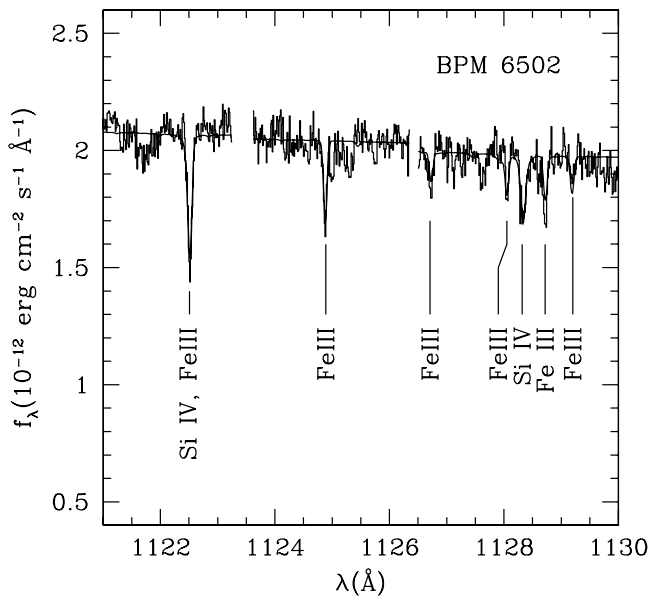

FIG. 7.—*FUSE* spectra showing the Fe III and Si IV (see Table 3) photospheric lines of BPM 6502 compared to the best-fit model. [*See the electronic edition of the Journal for a color version of this figure.*]

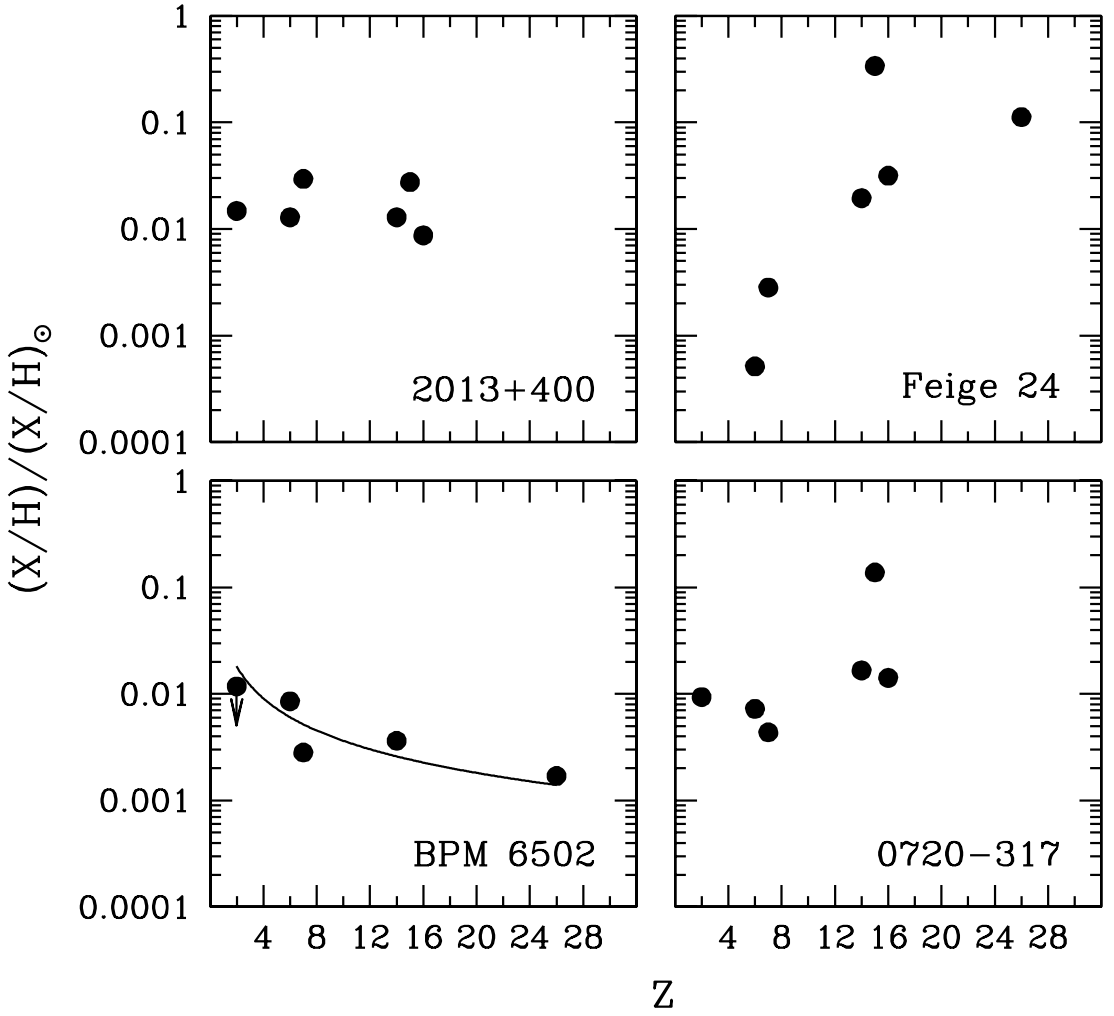

FIG. 8.—Measured abundances in Feige 24, EUVE J0720−317, BPM 6502, and EUVE J2013+400 relative to solar values (Asplund et al. 2005). The iron abundance in Feige 24 is from Vennes et al. (2000).

J0720−317 and J2013+400, but the absence of He I in medium-resolution spectra of BPM 6502 obtained by Kawka et al. (2000) places a limit on the helium abundance of $\log \mathrm{He/H} \lesssim -3$. Another interesting contrast emerges between Feige 24 and the three other binaries. The case of carbon is very instructive (see Fig. 6). The abundance of carbon is ≈1% solar in BPM 6502, EUVE J0720−317, and EUVE J2013+400, but it is ≈0.05% solar in Feige 24. Overall, Feige 24 presents an increased abundance toward larger atomic numbers. Although considerable scatter is present, one might conclude that, except for P in EUVE J0720−317, which appears somewhat more abundant, the abundances in BPM 6502, EUVE J0720−317, and EUVE J2013+400 are ≈0.2%–2% solar. Especially in the case of EUVE J0720−317 and J2013+400, this is in stark contrast with the abundance pattern noted in hot white dwarfs such as Feige 24 (see Vennes & Lanz 2001), which exhibit a yet unexplained trend showing increasing $(\mathrm{X/H})/(\mathrm{X/H})_\odot$ with Z. Although selective radiation pressure, which is very effective in the case of elements with a rich line spectrum (e.g., iron), plays an important role in white dwarf atmospheres, detailed comparisons between theory and observations are not satisfactory (Chayer et al. 1995). In the cases of EUVE J0720−317 and J2013+400, the presence of helium (normally not present in hot DA white dwarfs) and of a concentration of heavy elements at ≈1% solar concentration suggest that these elements are accreted from the close late-type companion via wind/mass loss. This wind/accretion scenario was explored in the case of the similar white dwarf plus late-type pair 1016−053 (Vennes et al. 1997a). The white dwarf in Feige 24, being in a wider binary ($P \approx 4.2$ days vs. ≲1 day) and considerably hotter, bears more resemblance to hot, isolated DA white dwarfs such as G191-B2B (Vennes & Lanz 2001).

It is possible to estimate the accretion rate expected to bring about the observed level of contamination. We adopt the accretion/diffusion model of Fontaine & Michaud (1979) as a possible explanation for the abundance pattern observed in BPM 6502. The model may also be tentatively applied to the abundance of light elements in EUVE J0720−317 and J2013+400. This simple scenario implies that elements are accreted onto the white dwarf surface from the late-type wind; elements heavier than hydrogen, the main atmospheric constituent, diffuse downward at a certain rate. The equilibrium abundance at a certain point in the atmosphere is given by

$$\frac{\mathrm{X/H}}{(\mathrm{X/H})_\odot} = \frac{\dot{M}}{\dot{M} + 4\pi R^2 \rho v_d}, \quad (1)$$

where X/H is the equilibrium abundance at that point, $(\mathrm{X/H})_\odot$ is the abundance in the red dwarf mass loss (presumably solar), $\dot{M}$ is the accretion rate onto the white dwarf, R is the white dwarf radius, ρ is the density in the atmosphere at the abundance

TABLE 9
DIFFUSION VELOCITIES AT $\tau_R = 2/3$

	v_d (cm s^{-1})	
ELEMENT	BPM 6502	EUVE J0720−317 and EUVE J2013+400
He II	...	0.003
C III	0.11	0.006
Fe III	0.51	...

measurement point, and v_d is the diffusion velocity at that same point. The white dwarf radius $R \approx 8.4 \times 10^8$ cm is given by the stellar model, and for the present demonstration we adopt the density ρ at a Rosseland depth $\tau_R = 2/3$ ($\rho = 7.3 \times 10^{-8}$ [for BPM 6502] and $\rho = 1.4 \times 10^{-7}$ g cm^{-3} [for EUVE J0720−317 and J2013+400]) from the atmospheric models discussed in § 4.1. We then calculate the diffusion velocity v_d at that location following the calculation of Fontaine & Michaud (1979). Table 9 gives the diffusion velocity of key elements at $\tau_R = 2/3$.

First, we examine the case of BPM 6502 and estimate the accretion rate onto the white dwarf atmosphere using the carbon abundance $X/H = 0.01(X/H)_\odot$ and the diffusion velocity from Table 9. A low rate of $\dot{M} = 1.1 \times 10^{-17}\ M_\odot\ \mathrm{yr}^{-1}$ is obtained. Next, assuming that a constant iron-to-carbon ratio (solar) is preserved in the wind and assuming the same accretion rate, we determine the predicted equilibrium abundance using the correct diffusion velocity for iron. The predicted iron abundance is lower than the carbon abundance by the factor $v_d(C)/v_d(Fe) = 0.2$. Indeed, the abundance of iron in BPM 6502 is about a factor of 5 lower than the carbon abundance. Figure 8 shows that the expected trend $(X/H)/(X/H)_\odot \propto A^{-1}$ (*solid line*), where A is the atomic weight, seems to apply to the case of BPM 6502. Renewed optical observations of BPM 6502 aimed at placing a tighter constraint on the helium abundance would also help verify this accretion/diffusion model. The diffusion velocity of singly ionized helium is similar to the velocity of doubly ionized carbon, which would imply a similar equilibrium abundance. However, the diffusion velocity of neutral helium is possibly a factor of 100 larger than for singly ionized species, which would considerably lower the equilibrium abundance of helium (Michaud et al. 1978).

A similar application of the accretion/diffusion model to the cases of EUVE J0720−317 and J2013+400 implies an accretion rate onto both white dwarfs of $\dot{M} = 1.8 \times 10^{-19}\ M_\odot\ \mathrm{yr}^{-1}$ (He) and $\dot{M} = 3.4 \times 10^{-19}\ M_\odot\ \mathrm{yr}^{-1}$ (C). The rates in the cases of EUVE J0720−317 and J2013+400 are markedly lower than in the case of BPM 6502, possibly because of their wider orbital separations or, hypothetically, their lower late-type mass-loss rates. Vennes et al. (1997a) determined a similar accretion rate onto the white dwarf 1016−053 of $\dot{M} = 8 \times 10^{-19}\ M_\odot\ \mathrm{yr}^{-1}$, based on their analysis of the helium abundance in the EUV photosphere of that star.

In summary, the observed abundance pattern in the atmosphere of BPM 6502 is consistent with an application of the accretion/diffusion model. The cases of EUVE J0720−317 and J2013+400 appear somewhat more complex, but their abundance patterns do bear some similarities to the pattern observed in BPM 6502. Feige 24 being in a wider binary than the other binaries studied in our sample, the abundance pattern may be dominated by ordinary diffusion, with possible effects due to radiative levitation and/or mass loss. In this context, it would be instructive to measure the iron abundance in the atmospheres of EUVE J0720−317 and J2013+400. Such measurements can be obtained using the far-UV lines of Fe IV and Fe V present at $\lambda \gtrsim 1300$ Å.

6. SUMMARY

We measured the white dwarf radial velocities in the close binary systems Feige 24, EUVE J0720−317, BPM 6502, and EUVE J2013+400 using *FUSE* spectra. Combined with previous optical studies of the binaries, we have updated the binary properties. Of the four systems, only EUVE J0720−317 is likely to come into contact within a Hubble time and is therefore a representative progenitor of the presently observed cataclysmic variables. We have also reanalyzed the optical data of Kawka et al. (2002) and Morales-Rueda et al. (2005) and showed that the correct orbital period of BPM 6502 is 0.3367849 ± 0.0000006 days and that the period reported by Morales-Rueda et al. (2005) should be discarded.

We measured the abundance of trace elements in the atmospheres of Feige 24, EUVE J0720−317, BPM 6502, and EUVE J2013+400 and found that the observed abundance pattern in BPM 6502 can be explained by steady accretion at a very low rate ($\sim 1 \times 10^{-17}\ M_\odot\ \mathrm{yr}^{-1}$). In the cases of EUVE J0720−317 and J2013+400 accretion from the secondary at much lower rates ($\sim 10^{-19}\ M_\odot\ \mathrm{yr}^{-1}$) can explain the observed abundances; however, the higher abundances of P in these stars cannot be explained by accretion from the secondary alone.

S. Vennes is grateful for the hospitality and support of the Astronomical Institute at Ondrejov Observatory. This work is supported by NASA grants NAG5-11717 and NAG5-6551. A. K. acknowledges support from the Grant Agency of the Czech Republic (GA ČR) 205/05/P186 and the Centre for Theoretical Astrophysics (LC06014). S. V. acknowledges support from the College of Science, Florida Institute of Technology. This work is based on observations made with the NASA-CNES-CSA *Far Ultraviolet Spectroscopic Explorer*. *FUSE* is operated for NASA by Johns Hopkins University under NASA contract NAS5-32985. This publication makes use of data products from the Two Micron All Sky Survey, which is a joint project of the University of Massachusetts and the Infrared Processing and Analysis Center, California Institute of Technology, funded by the National Aeronautics and Space Administration and the National Science Foundation.

REFERENCES

Asplund, M., Grevesse, N., & Sauval, A. J. 2005, in ASP Conf. Ser. 336, Cosmic Abundances as Records of Stellar Evolution and Nucleosynthesis, ed. T. G. Barnes III & F. N. Bash (San Francisco: ASP), 25
Barstow, M. A., O'Donoghue, D., Kilkenny, D., Burleigh, M. R., & Fleming, T. A. 1995a, MNRAS, 273, 711
Barstow, M. A., et al. 1995b, MNRAS, 272, 531
Benedict, G. F., et al. 2000, AJ, 119, 2382
Berger, D. H., et al. 2006, ApJ, 644, 475
Bessell, M. S. 1991, AJ, 101, 662
Bessell, M. S., & Brett, J. M. 1988, PASP, 100, 1134
Caillault, J.-P., & Patterson, J. 1990, AJ, 100, 825
Chayer, P., Oliveira, C., Dupuis, J., Moos, H. W., & Welsh, B. Y. 2003, in White Dwarfs, ed. D. de Martino, R. Silvotti, J.-E. Solheim, & R. Kalytis (NATO ASI Ser. B, 105; Dordrecht: Kluwer), 127
———. 2006, in ASP Conf. Ser. 348, Astrophysics in the Far Ultraviolet: Five Years of Discovery with FUSE, ed. G. Sonneborn, H. Moos, & B.-G. Andersson (San Francisco: ASP), 209
Chayer, P., Vennes, S., Pradhan, A. K., Thejll, P., Beauchamp, A., Fontaine, G., & Wesemael, F. 1995, ApJ, 454, 429
Cutri, R. M., et al. 2006, Explanatory Supplement to the 2MASS All Sky Data Release and Extended Mission Products (Pasadena: Caltech)
de Kool, M. 1992, A&A, 261, 188

Fontaine, G., & Michaud, G. 1979, ApJ, 231, 826
Gianninas, A., Dufour, P., & Bergeron, P. 2004, ApJ, 617, L57
Hébrard, G., Allard, N. F., Kielkopf, J. F., Chayer, P., Dupuis, J., Kruk, J. W., & Hubeny, I. 2003, A&A, 405, 1153
Holberg, J. B., Wesemael, F., & Basile, J. 1986, ApJ, 306, 629
Hubeny, I., & Lanz, T. 1995, ApJ, 439, 875
Kawka, A., & Vennes, S. 2006, ApJ, 643, 402
Kawka, A., Vennes, S., Dupuis, J., & Koch, R. 2000, AJ, 120, 3250
Kawka, A., Vennes, S., Koch, R., & Williams, A. 2002, AJ, 124, 2853
Kawka, A., Vennes, S., Schmidt, G. D., Wickramasinghe, D. T., & Koch, R. 2007, ApJ, 654, 499
Kirkpatrick, J. D., & McCarthy, D. W., Jr. 1994, AJ, 107, 333
Lallement, R., Ferlet, R., Lagrange, A. M., Lemoine, M., & Vidal-Madjar, A. 1995, A&A, 304, 461
Lanz, T., & Hubeny, I. 2003, ApJS, 146, 417
———. 2007, ApJS, 169, 83
López-Morales, M. 2007, ApJ, 660, 732
Maxted, P. F. L., Marsh, T. R., Moran, C., Dhillon, V. S., & Hilditch, R. W. 1998, MNRAS, 300, 1225
Michaud, G., Martel, A., & Ratel, A. 1978, ApJ, 226, 483
Moos, H. W., et al. 2000, ApJ, 538, L1
Morales-Rueda, L., Marsh, T. R., Maxted, P. F. L., Nelemans, G., Karl, C., Napiwotzki, R., & Moran, C. K. J. 2005, MNRAS, 359, 648
Orosz, J. A., Wade, R. A., Harlow, J. J. B., Thorstensen, J. R., Taylor, C. J., & Eracleous, M. 1999, AJ, 117, 1598
Rebassa-Mansergas, A., Gänsicke, B. T., Rodríguez-Gil, P., Schreiber, M. R., & Koester, D. 2007, MNRAS, 382, 1377
Ritter, H. 1986, A&A, 169, 139
Sahnow, D. J., et al. 2000a, Proc. SPIE, 4013, 334
———. 2000b, Proc. SPIE, 4139, 131
Schreiber, M. R., & Gänsicke, B. T. 2003, A&A, 406, 305
Tappert, C., Gänsicke, B. T., Schmidtobreick, L., Mennickent, R. E., & Navarrete, F. P. 2007, A&A, 475, 575
Thorstensen, J. R., Charles, P. A., Margon, B., & Bowyer, S. 1978, ApJ, 223, 260
Thorstensen, J. R., Vennes, S., & Shambrook, A. 1994, AJ, 108, 1924
Vennes, S., Chayer, P., Dupuis, J., & Lanz, T. 2005, in ASP Conf. Ser. 334, 14th European Workshop on White Dwarfs, ed. D. Koester & S. Moehler (San Francisco: ASP), 185
———. 2006, ApJ, 652, 1554
Vennes, S., Dupuis, J., Bowyer, S., & Pradhan, A. K. 1997a, ApJ, 482, L73
Vennes, S., & Lanz, T. 2001, ApJ, 553, 399
Vennes, S., Polomski, E. F., Lanz, T., Thorstensen, J. R., Chayer, P., & Gull, T. R. 2000, ApJ, 544, 423
Vennes, S., Thejll, P., Génova-Galvan, R., & Dupuis, J. 1997b, ApJ, 480, 714
Vennes, S., & Thorstensen, J. R. 1994a, ApJ, 433, L29
———. 1994b, AJ, 108, 1881
Vennes, S., Thorstensen, J. R., & Polomski, E. F. 1999, ApJ, 523, 386
Wade, R. A., & Horne, K. 1988, ApJ, 324, 411
Wood, M. A. 1995, in White Dwarfs, ed. D. Koester & K. Werner (Berlin: Springer), 41